Available online at www.sciencedirect.com
ScienceDirect
C. R. Geoscience 340 (2008) 223–232
COMPTES RENDUS GEOSCIENCE
http://france.elsevier.com/direct/CRAS2A/

Geochemistry (Geochronology)

U–Pb Shrimp-RG zircon ages of Variscan igneous rocks from the Guilleries massif (NE Iberia pre-Mesozoic basement). Geological implications

Francisco José Martínez [a,*], Joan Reche [a], Alexander Iriondo [b,c]

[a] *Departament de Geologia, Universitat Autònoma de Barcelona, 08193 Bellaterra, Spain*
[b] *Centro de Geociencias, Universidad Nacional Autónoma de México, Campus Juriquilla, C.P. 76230 Juriquilla, Querétaro, Mexico*
[c] *Department of Geological Sciences, University of Colorado at Boulder, Boulder, Colorado 80309, USA*

Received 28 June 2007; accepted after revision 10 December 2007
Available online 4 March 2008

Presented by Ždenek Johan

Abstract

One diorite sheet, syntectonic with the dominant D2 foliation in the Guilleries massif, 50 km south of the Variscan Pyrenean axial zone, has provided an U–Pb age of 323.6 ± 2.8 Ma, one of the oldest in that part of the Variscan basement. This age seems to be the same as that of the sillimanite-grade syn-D2 metamorphism in the deepest part of the massif; it is clearly separated from that obtained in three syn-extensional D3 leucogranite veins (305.3 ± 1.9; 301.5 ± 1.7; 299.0 ± 2.3 Ma) and the coeval biotite granites (305.9 ± 1.5 Ma). The leucogranites are 20 Ma younger than the syn-D2 diorite and the sillimanite-grade metamorphism. They are considered the melting-induced products in the host rocks, at a deeper level than that of the present outcropping of the mantle-related biotite granites during the extensional collapse (D3) of the chain in the Lower Stephanian. ***To cite this article: F.J. Martínez et al., C. R. Geoscience 340 (2008).***

Résumé

Datations U–Pb par la méthode Shrimp sur zircons de roches ignées varisques du massif des Guilleries (socle pré-Mésozoïque du Nord-Est de l'Espagne). Implications géologiques. La datation U–Pb d'une intrusion laminaire dioritique syntectonique de la foliation dominante D2 (qu'elle soit d'origine compressive ou extensive), dans le massif des Guilleries, situé 50 km au sud de la zone axiale varisque pyrénéenne, indique un âge de cristallisation de 323,6 ± 2,8 Ma, un des plus anciens obtenu dans cette région du socle varisque. Cet âge doit correspondre à l'âge du métamorphisme à sillimanite syn-D2 dans les parties profondes du massif ; il est nettement distinct des âges obtenus sur trois veines de leucogranite syn-extension D3 (305,3 ± 1,9 ; 301,5 ± 1,7 ; 299,0 ± 2,3 Ma) et un granite à biotite contemporain (305,9 ± 1,5 Ma). Ces leucogranites postdatent de 20 Ma la diorite syn-D2 et le métamorphisme à sillimanite. Ils sont considérés comme étant les produits de fusion de l'encaissant, induits par la mise en place en profondeur des granites à biotite d'influence mantellique au cours de

* Corresponding author.
E-mail address: francisco.martinez@uab.es (F.J. Martínez).

1631-0713/$ – see front matter
doi:10.1016/j.crte.2007.12.006

l'extension (D3), par effondrement gravitaire de la chaîne au Stéphanien inférieur. ***Pour citer cet article : F.J. Martínez et al., C. R. Geoscience 340 (2008).***

Keywords: Shrimp ages; Variscan intrusions; NE Iberia; Diorite; Leucogranite; Biotite granite

Mots clés : Datations Shrimp ; Intrusions Varisques ; Nord-Est de l'Espagne ; Diorite ; Leucogranite ; Granite à biotite

1. Geological setting and problems to be solved

1.1. Context

The available radiometric data on the timing and relationships of Variscan magmatism and metamorphism in the Northeast Iberian massifs suggest a late, Upper-Carboniferous age for these events [1] compared for instance to Northwest Iberia [8], which occupies an equivalent position in the Chain, where syn-metamorphic granitoids are older [3]. In this regard, the Guilleries massif provides a good example of a close relationship between magmatism and medium- to high-grade metamorphism [11] to further evaluate this model. The dating of the Variscan intrusions would also help to know the relative age of the two main pervasive foliations found in the more metamorphic part of the massif [2]: S1 (D1) is the oldest cleavage (a slaty cleavage in low-grade areas), which becomes refolded by a strong syn-metamorphic S2 (D2) foliation, whose transpressive or transtensive nature is the subject of debate in different parts of the Chain. A shear-band style, extensional deformation D3 occurs in the studied massif that is linked to retrogression [11].

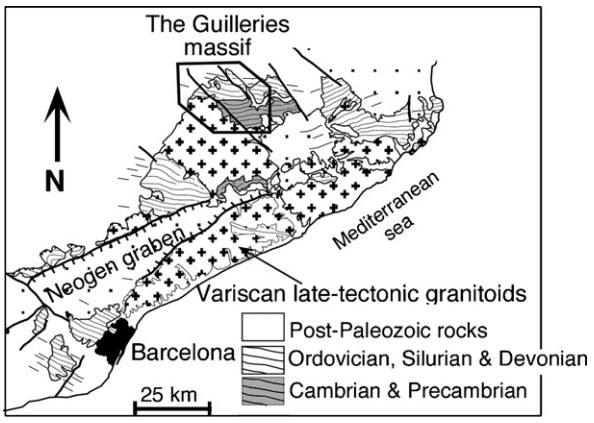

Fig. 1. Sketch of the Catalonian Coastal Ranges location of the Guillerias massif.

Fig. 1. Schéma de localisation du massif des Guilleries dans les Chaînes côtières catalanes.

The Guilleries massif (Fig. 1) is comparable to the Canigó and Albera Variscan massifs [5,15] of the Pyrenean axial zone, but located approximately 50 km south of them. The massif is divided from south to north into three blocks: Osor, Susqueda, and Sant Martí (A, B, and C in Fig. 2). These blocks are separated by NE–SW-striking normal faults that sink their northern limbs, causing the deeper, more metamorphic, and richer in igneous intrusions Osor block to outcrop in the southern part of the massif.

1.2. Leucogranites in the Osor block

The Osor block, bounded to the south by a large mass of biotite granites, is intruded by a large number of leucogranite bodies and associated aplites and

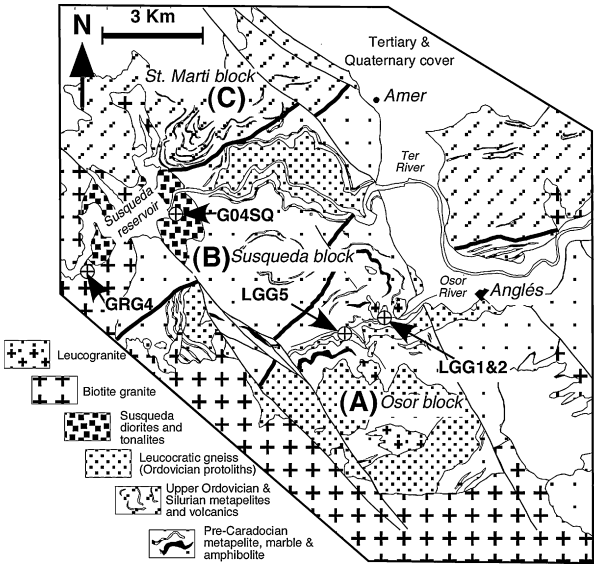

Fig. 2. Geology of the massif, with the location of the Osor, Susqueda, and St. Martí blocks (**A**, **B**, and **C**). Bold lines are normal faults, displaced by Neogene faults, which sink the northern blocks and cause the deepest rocks (Osor area) to outcrop to the south.

Fig. 2. Géologie du massif, avec la situation des zones d'Osor, Susqueda et St. Martí (**A**, **B** et **C**). Les lignes en gras correspondent aux failles normales qui enfoncent le bloc nord, faisant affleurer au sud (zone d'Osor) les niveaux les plus profonds. Les failles normales sont recoupées par des failles néogènes.

Table 1
Isotopic data for individual zircons from analysed samples

Tableau 1
Données isotopiques par zircon des échantillons analysés

Spot name	Comments Core/Rim?	Common ^{206}Pb (%)	U (ppm)	Th (ppm)	Th/U	$^{238}U/^{206}Pb$[a]		error (%)	$^{207}Pb/^{206}Pb$[a]		error (%)	$^{206}Pb/^{238}U$[b]		error (%)	$^{206}Pb/^{238}U$[b] Age (Ma)		Error (Ma)
Sample LGG5 Osor leucogranite vein (Guilleries massif) (UTM: 466.345–4.644.509; Zone 31N–ED50) Mount Alex–11																	
LGG5–8	Core	0.33	216	128	0.59	21.1113	±	1.0765	0.0549	±	2.0534	0.0472	±	0.0005	**297.4**	±	**3.2**
LGG5–6	Core	0.02	395	222	0.56	21.0965	±	0.9953	0.0525	±	1.8166	0.0474	±	0.0005	**298.5**	±	**2.9**
LGG5–9	Rim	0.10	339	63	0.18	21.0399	±	0.9617	0.0531	±	1.6690	0.0475	±	0.0005	**299.0**	±	**2.9**
LGG5–4	Rim	0.01	541	23	0.04	21.0249	±	0.8701	0.0524	±	1.3103	0.0476	±	0.0004	**299.5**	±	**2.6**
LGG5–5	Core	0.09	467	262	0.56	20.9334	±	1.3944	0.0531	±	1.4139	0.0477	±	0.0007	**300.5**	±	**4.1**
LGG5–11	Rim	0.00	317	160	0.51	20.8953	±	0.9735	0.0524	±	1.7318	0.0479	±	0.0005	**301.4**	±	**2.9**
LGG5–7	Rim	0.55	672	118	0.18	20.7393	±	0.8496	0.0568	±	1.1736	0.0480	±	0.0004	**301.9**	±	**2.5**
LGG5–2	Core/Rim	0.25	283	144	0.51	20.7206	±	1.0071	0.0544	±	1.8131	0.0481	±	0.0005	**303.1**	±	**3.0**
LGG5–10	Core/Rim	0.05	633	169	0.27	20.7372	±	0.8510	0.0528	±	1.2106	0.0482	±	0.0004	**303.5**	±	**2.6**
LGG5–1	Core	0.24	332	63	0.19	20.6071	±	0.9657	0.0544	±	1.6652	0.0484	±	0.0005	**304.7**	±	**2.9**
LGG5–3	Rim	0.33	252	93	0.37	20.4173	±	1.0632	0.0552	±	2.0003	0.0488	±	0.0005	**307.2**	±	**3.2**
LGG5–12	Core	0.04	340	46	0.13	20.3016	±	0.9855	0.0529	±	1.7677	0.0492	±	0.0005	309.8	±	3.0
									(MSWD = 0.94)			Mean $^{206}Pb/^{238}U$ age =			**301.5**	±	**1.7**
Sample LGG1 Osor leucogranite vein (Guilleries massif) (UTM: 467.211–4.644.698; Zone 31N–ED50) Mount Alex–32bis																	
LGG1–13	Core	0.12	435	6	0.02	20.5961	±	0.6305	0.0534	±	1.8819	0.0485	±	0.0003	305.3	±	1.9
LGG1–10	Core/Rim	–0.04	392	14	0.04	20.1535	±	0.6219	0.0523	±	1.8767	0.0496	±	0.0003	312.3	±	1.9
LGG1–15	Core	1.22	356	197	0.57	13.8227	±	0.6432	0.0657	±	1.5615	0.0715	±	0.0005	444.9	±	2.9
LGG1–4	Core	0.12	381	228	0.62	13.6234	±	0.5721	0.0571	±	1.4873	0.0733	±	0.0004	456.1	±	2.6
LGG1–12	Core	2.13	469	93	0.21	12.2462	±	0.5111	0.0744	±	1.1925	0.0799	±	0.0005	495.6	±	2.8
LGG1–8	Core	1.17	335	78	0.24	11.7901	±	0.5976	0.0672	±	1.3843	0.0838	±	0.0005	518.9	±	3.2
LGG1–2	Rim/Core	0.33	561	41	0.08	11.6861	±	0.4537	0.0606	±	1.1183	0.0853	±	0.0004	527.6	±	2.4
LGG1–5	Core	–0.12	223	113	0.52	9.8350	±	0.7083	0.0597	±	1.6403	0.1018	±	0.0007	624.9	±	4.4
LGG1–1	Core	2.52	130	113	0.90	7.9227	±	0.8744	0.0850	±	1.6393	0.1230	±	0.0012	see Table 2		
LGG1–3	Core	0.60	121	60	0.51	8.0348	±	0.9118	0.0693	±	1.8701	0.1237	±	0.0012	see Table 2		
LGG1–7	Core	11.74	136	108	0.82	6.4635	±	0.8148	0.1637	±	1.0006	0.1366	±	0.0026	see Table 2		
LGG1–11	Core	0.34	275	52	0.20	6.3843	±	0.5812	0.0730	±	1.0874	0.1561	±	0.0010	see Table 2		
LGG1–9	Core	3.94	583	163	0.29	3.3061	±	0.3501	0.1352	±	0.3978	0.2906	±	0.0019	see Table 2		
LGG1–14	Core	9.04	152	121	0.82	3.0936	±	0.7272	0.1802	±	0.9569	0.2940	±	0.0045	see Table 2		
LGG1–6	Core	0.36	270	52	0.20	3.0553	±	0.5778	0.1144	±	0.6643	0.3261	±	0.0021	see Table 2		
Sample LGG2 Osor leucogranite vein (Guilleries massif) (UTM: 467.535–4.644.503; Zone 31N–ED50) Mount Alex–32bis																	
LGG2–8	Rim. High ^{206}Pb	48.94	1235	195	0.16	29.9221	±	0.3745	0.4371	±	3.1664	0.0171	±	0.0021	109.1	±	13.6
LGG2–5	Core. High ^{206}Pb	62.60	1331	139	0.11	11.8311	±	0.2978	0.5503	±	0.3138	0.0316	±	0.0067	200.6	±	41.6
LGG2–2	Rim. High ^{206}Pb	13.78	799	80	0.10	18.8891	±	0.4477	0.1627	±	2.2206	0.0456	±	0.0010	287.7	±	6.0
LGG2–11	Core	0.36	183	41	0.23	21.2292	±	0.9279	0.0551	±	2.7292	0.0469	±	0.0004	**295.7**	±	**2.8**
LGG2–7	Core/Rim	0.17	547	484	0.91	21.2561	±	0.5448	0.0536	±	1.6383	0.0470	±	0.0003	**295.9**	±	**1.6**
LGG2–9	Core/Rim	0.74	354	175	0.51	20.9708	±	0.6705	0.0583	±	1.9395	0.0473	±	0.0003	**298.1**	±	**2,0**
LGG2–4	Rim	2.69	174	97	0.58	20.5198	±	1.0418	0.0739	±	2.6181	0.0474	±	0.0005	**298.7**	±	**3,3**

Table 1 (*Continued*)

Spot name	Comments Core/Rim?	Common ^{206}Pb (%)	U (ppm)	Th (ppm)	Th/U	$^{238}U/^{206}Pb$[a]		error (%)	$^{207}Pb/^{206}Pb$[a]		error (%)	$^{206}Pb/^{238}U$[b]		error (%)	$^{206}Pb/^{238}U$[b] Age (Ma)		Error (Ma)
LGG2–1	Core/Rim	0.30	387	113	0.30	20.9135	±	0.6743	0.0547	±	1.9756	0.0477	±	0.0003	**300.2**	±	**2,0**
LGG2–6	Core/Rim	–0.13	312	88	0.29	20.8870	±	0.7332	0.0513	±	2.2282	0.0479	±	0.0004	**301.8**	±	**2,2**
LGG2–12	Core	0.37	189	107	0.58	20.7752	±	0.9472	0.0554	±	2.7878	0.0480	±	0.0005	**302.0**	±	**2,9**
LGG2–3	Core/Rim	0.28	407	274	0.70	20.7506	±	0.7315	0.0547	±	1.9021	0.0481	±	0.0004	**302.6**	±	**2,2**
LGG2–10	Core	0.53	122	54	0.46	20.2795	±	1.1277	0.0568	±	3.2665	0.0490	±	0.0006	308.7	±	3,5
									(MSWD = 1.6)			Mean $^{206}Pb/^{238}U$ age =			299.0	±	2.3
Sample GRG4 Susqueda biotite granite (Guilleries massif) (UTM: 457.824–4.645.624; Zone 31N–ED50) Mount Alex–11																	
GRG4–7	Rim	0.04	757	98	0.13	21.1857	±	0.8310	0.0526	±	1.3251	0.0472	±	0.0004	297.2	±	2,4
GRG4–13	Rim	1.29	1369	173	0.13	20.5052	±	0.7754	0.0627	±	1.1122	0.0481	±	0.0004	**303.1**	±	**2,4**
GRG4–10	Rim	0.04	1227	168	0.14	20.7278	±	0.7829	0.0527	±	0.8665	0.0482	±	0.0004	**303.6**	±	**2,3**
GRG4–5	Rim	0.12	1143	108	0.09	20.7067	±	0.7915	0.0534	±	0.9116	0.0482	±	0.0004	**303.7**	±	**2,4**
GRG4–14	Rim	0.05	550	199	0.36	20.6358	±	0.8747	0.0529	±	1.3163	0.0484	±	0.0004	**304.9**	±	**2,6**
GRG4–12	Rim	–0.04	567	85	0.15	20.6436	±	0.8690	0.0521	±	1.2997	0.0485	±	0.0004	**305.1**	±	**2,6**
GRG4–4	Core/Rim	0.13	508	241	0.48	20.5586	±	0.8900	0.0535	±	1.3730	0.0486	±	0.0004	**305.8**	±	**2,7**
GRG4–1	Rim	0.05	1182	200	0.17	20.5593	±	0.7899	0.0529	±	0.9054	0.0486	±	0.0004	**306.0**	±	**2,4**
GRG4–3	Rim	–0.03	939	63	0.07	20.5214	±	0.8120	0.0523	±	1.0334	0.0487	±	0.0004	**306.8**	±	**2,5**
GRG4–2	Rim	12.48	501	116	0.23	17.9587	±	0.8748	0.1527	±	4.0862	0.0487	±	0.0011	**306.8**	±	**6,6**
GRG4–8	Rim	0.12	362	195	0.54	20.4359	±	0.9698	0.0535	±	1.6895	0.0489	±	0.0005	**307.6**	±	**3,0**
GRG4–9	Rim	0.00	647	122	0.19	20.3365	±	0.8579	0.0525	±	1.2478	0.0492	±	0.0004	**309.5**	±	**2,6**
GRG4–11	Rim	–0.14	501	128	0.25	20.2522	±	0.8910	0.0515	±	1.4028	0.0494	±	0.0004	**311.1**	±	**2,7**
									(MSWD = 1.5)			Mean $^{206}Pb/^{238}U$ age =			**305.9**	±	**1.5**
Sample G04SQ Susqueda diorite (Guilleries massif) (UTM: 460.601–4.647.607; Zone 31N–ED50) Mount Alex–19																	
G04SQ–5	Core	0.10	99	43	0.44	19.8408	±	1.2136	0.0535	±	3.8553	0.0504	±	0.0006	**316.7**	±	**3,9**
G04SQ–8	Core	0.22	217	125	0.58	19.6175	±	0.8078	0.0546	±	2.2763	0.0509	±	0.0004	**319.8**	±	**2,6**
G04SQ–4	Core. High U	0.10	534	344	0.64	19.6324	±	0.5122	0.0536	±	1.4529	0.0509	±	0.0003	320.0	±	1,6
G04SQ–1	Core	0.00	266	153	0.58	19.5672	±	0.6485	0.0528	±	2.1135	0.0511	±	0.0003	**321.3**	±	**2,1**
G04SQ–9	Core	–0.25	286	172	0.60	19.4860	±	0.6979	0.0509	±	2.0145	0.0514	±	0.0004	**323.4**	±	**2,3**
G04SQ–10	Core	–0.15	393	102	0.26	19.4410	±	0.5969	0.0517	±	1.7280	0.0515	±	0.0003	**323.8**	±	**1,9**
G04SQ–6	Core	–0.05	143	54	0.38	19.3926	±	0.9860	0.0525	±	2.8121	0.0516	±	0.0005	**324.3**	±	**3,2**
G04SQ–7	Core	–0.17	317	204	0.64	19.3199	±	0.6685	0.0516	±	1.9237	0.0518	±	0.0004	**325.9**	±	**2,2**
G04SQ–2	Core	0.31	113	55	0.49	18.9537	±	1.2297	0.0555	±	3.0884	0.0526	±	0.0007	**330.4**	±	**4,1**
G04SQ–3	Core	0.07	101	34	0.33	18.9045	±	1.1657	0.0536	±	3.2783	0.0529	±	0.0006	**332.1**	±	**3,9**
									(MSWD = 1.9)			Mean $^{206}Pb/^{238}U$ age =			**323.6**	±	**2.8**

Individual zircon ages in bold were used to calculate the weighted average $^{206}Pb/^{238}U$ age and its MSWD (Mean Square of Weighted Deviates).
All errors given are at the 1 σ level except for the weighted average $^{206}Pb/^{238}U$ age, reported at 2σ.

[a] Uncorrected atomic ratios.

[b] Atomic ratios and ages corrected for initial Pb using the amount of ^{207}Pb.

pegmatites, which are most commonly between 1 to 10 m thick and less than 50 m long, although a few bodies (the only ones represented in Fig. 2) may extend up to 1 km^2. These leucogranites crosscut the host-rock syn-metamorphic dominant fabric (S2), but show different degrees of deformation. They have been interpreted as pre- to syntectonic with the late extensional event (D3) [11], and are intruded in sillimanite-grade metapelites with interlayered metapsammites, calc-silicates, amphibolites, and orthogneisses.

The dating of these leucogranites should therefore provide an upper age for both the sillimanite-grade metamorphism and the strong syn-metamorphic D2. It would also give an indication of whether D2 and D3 are related or separated in time.

The field relationships of the leucogranites and the large mass of mafic and intermediate enclave-bearing biotite granite that forms the southwestern boundary of the Guilleries massif (Fig. 2) are not clear, due to poor outcropping conditions; however, they have been considered older than the biotite granites [2]. As a result, the dating of the biotite granites should clarify their mutual temporal relations.

1.3. Diorites and tonalites in the Susqueda block

The Susqueda block, formed by metapelites and psammites with some quartzite layers, is located to the north of the Osor block, on the hanging wall of a normal fault separating both of them (Fig. 2). In contrast with the Osor block, leucogranites are almost absent here, the rocks are significantly less recrystallized, and the metamorphic grade in the metapelites only reaches andalusite–cordierite grade.

A subconcordant intrusion, consisting mainly of hornblende–biotite diorites and tonalites (Fig. 2), which occurs in the western part of the Susqueda block, induced melting at approximately 3 kbar and 760 °C in the Cambro-Ordovician metapelites [12]. This intrusion is concordant with regional foliation S2 at map scale, although at outcrop scale, it crosscuts S1 and is folded by D2. It is considered to be syn-tectonic with D2, since the wavelength of D2 microfolds in the contact is controlled by recrystallization, such that hornfelsic lens-shaped bodies occur, in which the D2 microfolds are less tight than they are outside. The dating of the Susqueda intrusion must provide an age for the thermal pulse it represents within the Susqueda block. It would also constrain the age of D2 and facilitate the determination of whether or not there is an age gap between this intrusion and that of the Osor leucogranites.

Table 2
U–Th–Pb analytical data for zircon grains with ages older than 700 Ma

Tableau 2
Données analytiques U–Th–Pb des grains de zircon d'âges supérieurs à 700 Ma

Spot name	Comments Core/Rim?	Common ^{206}Pb (%)	U (ppm)	Th (ppm)	Th/U	^{207}Pb/^{206}Pb[a]	error (%)	^{207}Pb/^{235}U[a]	error (%)	^{206}Pb/^{238}U[a]	error (%)	error correl.	% discor.[b]	^{207}Pb/^{206}Pb Age (Ma)	error (Ma)
Sample LGG1 Osor leucrogranite vein (Guilleries massif) (UTM: 467,211–4,644,698; Zone 31N-ED50) Mount Alex-32bis															
LGG1–1	Core	2.52	130	113	0.90	0.0660	±	7.1	1.12	± 7.2	0.1233	± 1.0	0.138	7	806	±	148
LGG1–3	Core	0.60	121	60	0.51	0.0673	±	2.9	1.15	± 3.1	0.1242	± 0.9	0.301	12	846	±	61
LGG1–11	Core	0.34	275	52	0.20	0.0725	±	1.2	1.56	± 1.3	0.1565	± 0.6	0.445	7	999	±	24
LGG1–7	Core	11.74	136	108	0.82	0.1002	±	11.3	1.97	± 11.4	0.1423	± 1.2	0.106	90	1628	±	210
LGG1–6	Core	0.36	270	52	0.20	0.1144	±	0.7	5.16	± 0.9	0.3273	± 0.6	0.656	2	1870	±	12
LGG1–9	Core	3.94	583	163	0.29	0.1341	±	0.5	5.58	± 0.6	0.3021	± 0.4	0.609	26	2152	±	8
LGG1–14	Core	9.04	152	121	0.82	0.1683	±	2.3	7.39	± 2.5	0.3185	± 0.8	0.335	43	2541	±	39

[a] Atomic ratios corrected for initial Pb using the amount of ^{204}Pb and the corresponding average earth values from Stacey and Kramers [14]. All errors given are at the 1 σ level.
[b] Degree of discordance, percentage of the distance that the analysis lies along a chord from its extrapolated intersection with concordia (corresponding to its ^{207}Pb/^{206}Pb age) to the origin at 0 Ma.

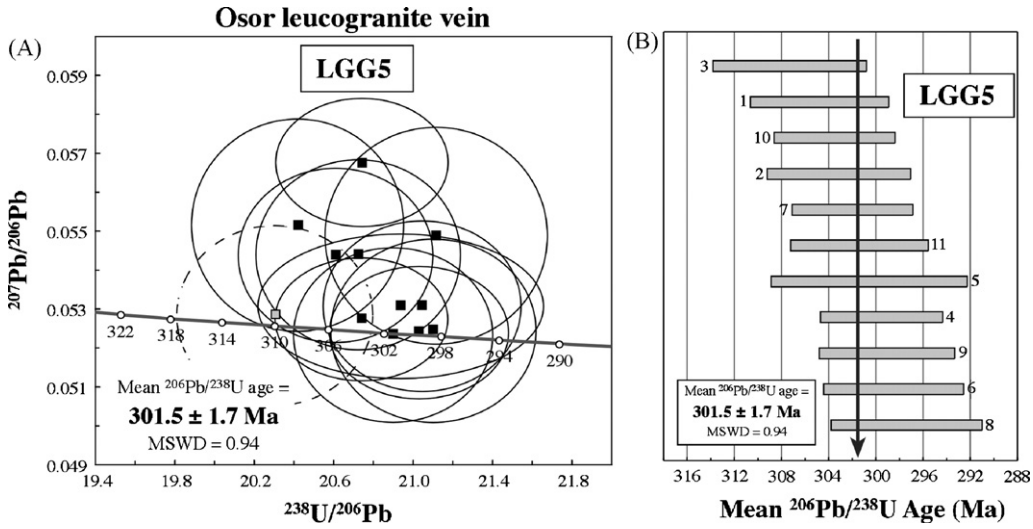

Fig. 3. U–Pb Shrimp-RG zircon geochronology data for the Osor leucogranite vein (LGG5). (**a**) Tera–Wasserburg U–Pb concordia plot with solid-line ellipses with black square centres representing the data used for age calculation. Dotted-line error ellipse with a gray square centre represents a data point excluded from age calculation. (**b**) Weighted mean $^{206}Pb/^{238}U$ age graph with calculated age and MSWD. Here and elsewhere, all the U–Pb data in the different graphs (ellipses and boxes) are plotted at the 2σ level of precision.

Fig. 3. Résultats des analyses géochronologiques U–Pb Shrimp-RG sur zircon d'une veine des leucogranites d'Osor (LGG5). (**a**) Âge moyen obtenu à partir des rapports isotopiques dans le diagramme concordia U–Pb de Tera–Wasserburg. Carrés noirs : données utilisées pour le calcul de l'âge. Carrés gris : données exclues pour le calcul de l'âge. Ellipses : précision 2σ. Le type de représentation est le même dans les diagrammes suivants. (**b**) Diagramme des intervalles d'âges obtenus pour les différents zircons et âge moyen pondéré $^{206}Pb/^{238}U$.

2. Sampling and U–Pb zircon dating

Three leucogranites from the Osor area and one biotite granite and one diorite from the Susqueda area in the Guilleries massif (see locations in Fig. 2) have been dated with U–Pb zircon geochronology using the Shrimp-RG instrument at Stanford University (See Appendix A for analytical techniques). Isotopic data were reduced and plotted using the Squid and IsoplotEx programs of Ludwig [6,7] and are presented in Tables 1 and 2. Uncorrected U–Pb zircon spot data are projected to the Tera–Wasserburg Concordia diagrams (Figs. 3–7)

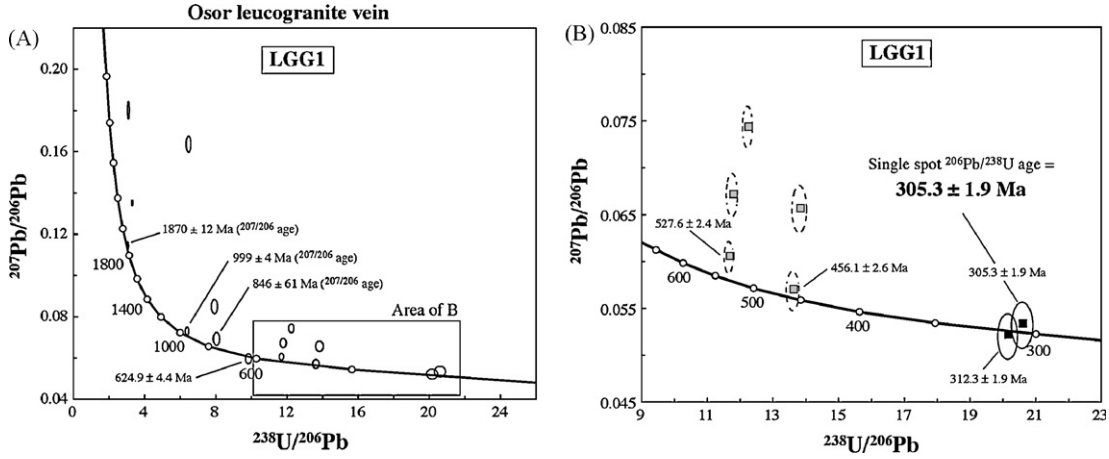

Fig. 4. U–Pb Shrimp-RG zircon geochronology data for the Osor leucogranite vein (LGG1). (**a**) Tera–Wasserburg U–Pb concordia plot with all data showing the older inherited grains with their $^{207}Pb/^{206}Pb$ ages. (**b**) Concordia plot close-up showing the youngest zircon grains.

Fig. 4. Résultats géochronologiques sur zircon d'une veine des leucogranites d'Osor LGG1. (**a**) Représentation de toutes les données obtenues dans le diagramme concordia U–Pb de Tera–Wasserburg, montrant les grains hérités les plus vieux et les âges correspondants. (**b**) Détail de (**a**), montrant les grains les plus jeunes.

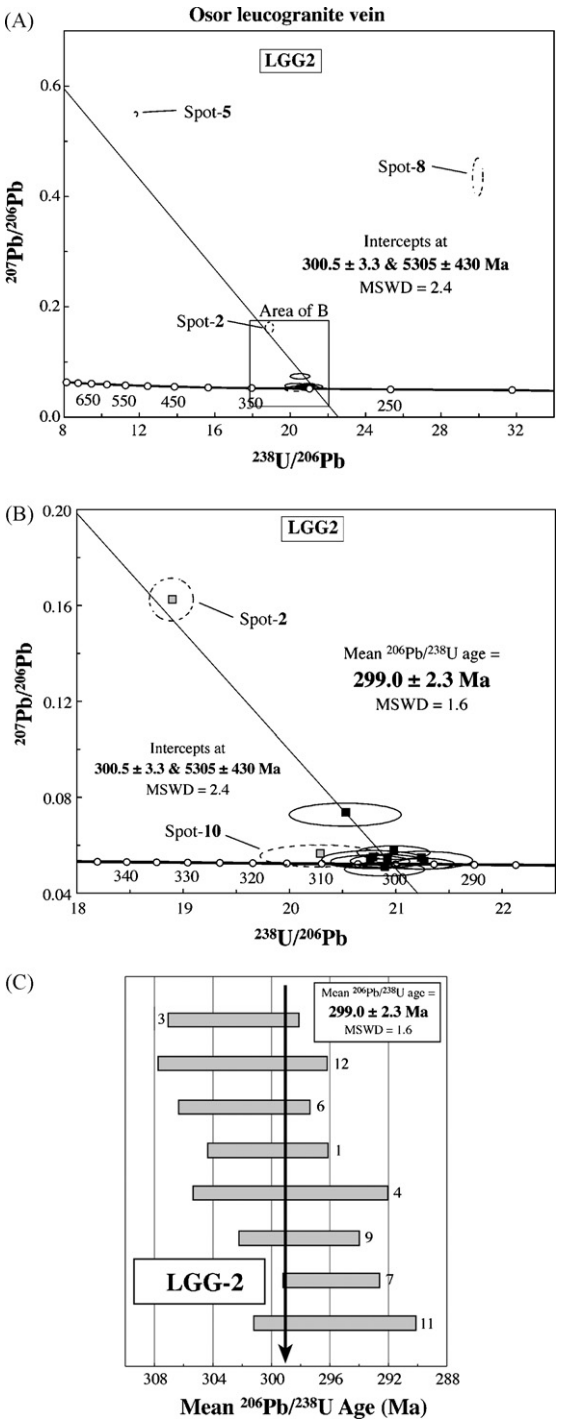

Fig. 5. U–Pb Shrimp–RG zircon geochronology data for the Osor leucogranite vein (LGG2). (**a**) Tera–Wasserburg U–Pb concordia plot with all data points showing upper and lower concordia intercepts. (**b**) Concordia plot close-up for the most concordant zircon grains. Solid-line ellipses with black square centres represent the data used for $^{206}Pb/^{238}U$ age calculation. The dotted-line error ellipses with gray square centres (Spot-2, 5, 8 & 10) represent data points excluded from age calculation. (**c**) Weighted mean $^{206}Pb/^{238}U$ age graph with calculated age and MSWD.

Fig. 5. Résultats géochronologiques sur zircons d'une veine des leucogranites d'Osor LGG2. (**a**) Représentation de toutes les données obtenues dans le diagramme concordia U–Pb de Tera–Wasserburg, montrant les intersections supérieures et inférieures. (**b**) Détail de la projection des zircons les plus concordants. Les données 2, 5, 8 & 10 ont été exclues du calcul d'âge. (**c**) Diagramme des intervalles d'âges obtenus pour les différents zircons et âge moyen pondéré $^{206}Pb/^{238}U$.

along a model common-Pb line after Stacey and Kramers [14]. For most samples, a preferred weighted mean $^{206}Pb/^{238}U$ age is calculated at 2-sigma level of precision and shown in a diagram adjacent to the Tera–Wasserburg diagrams (Figs. 3–7).

The three leucogranites from the Osor area are medium to fine-grained, muscovite-rich, two-mica granites and were collected from subconcordant veins, less than 20 cm thick, intrusive in the metasediments along the Osor River route GI-642. Their UTM (Zone 31N-ED50) coordinates are LGG1: 467211 4644698; LGG2: 467535 4644503; LGG5: 466345 4644509). U–Pb zircon data for sample LGG5, plotted in a Tera–Wasserburg concordia (Fig. 3a), shows that 11 data points, collected form a concordant array, gave a mean $^{206}Pb/^{238}U$ age of 301.5 ± 1.7 Ma (Fig. 3b; MSWD = 0.94; 2-sigma). Individual zircon ages used to calculate this $^{206}Pb/^{238}U$ age are shown in bold in Table 1. Only one data point (spot-12; dotted-line error ellipse in Fig. 3a) for this sample was excluded from the calculation because it is statistically older, and may represent an area of the zircon with some degree of inheritance. We interpret this mean $^{206}Pb/^{238}U$ age as the time of crystallization for this leucogranite vein.

Zircon data for leucogranite sample LGG1 are more complex and indicate the presence of abundant zircon inheritance with both Precambrian (Fig. 4a; $^{207}Pb/^{206}Pb$ ages) and Palaeozoic ages (Fig. 4b). Individual zircon ages are shown in Tables 1 and 2. There are two concordant data points (Fig. 4b) close to the age obtained for leucogranite samples LGG5 and LGG2 (discussed below), but the youngest single-spot $^{206}Pb/^{238}U$ age at 305.3 ± 1.9 Ma (1-sigma) is our best approximation for the crystallization age of this leucogranite sample. We acknowledge the limitation of this age constraint for leucogranite LGG1.

Leucogranite sample LGG2, collected only few hundred metres away from LGG1, has a zircon population with much better U–Pb behaviour; there is no evidence of the presence of inheritance comparing to sample LGG1. In this case, a Tera–Wasserburg

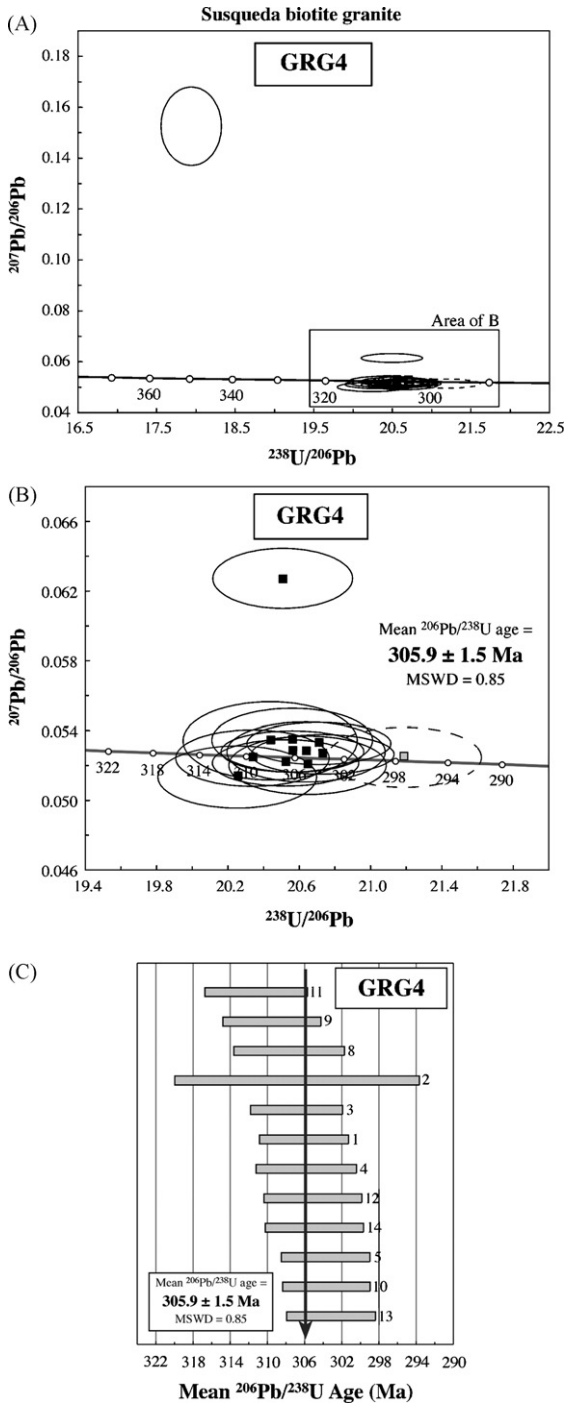

Fig. 6. U–Pb Shrimp-RG zircon geochronology data for the biotite granite GRG4. (**a**) Tera–Wasserburg U–Pb concordia plot with all data points. (**b**) Concordia plot close-up for the most concordant zircon grains. Solid-line ellipses with black square centres represent the data used for $^{206}Pb/^{238}U$ age calculation. The dotted-line error ellipse with a gray square centre represents a data point excluded from the age calculation. (**c**) Weighted mean $^{206}Pb/^{238}U$ age graph with calculated age and MSWD.

Concordia plot (Fig. 5a & b) shows that eight data points collected from a concordant array gave a mean $^{206}Pb/^{238}U$ age of 299.0 ± 2.3 Ma (Fig. 5c; MSWD = 1.6; 2-sigma). Individual zircon ages used to calculate the preferred $^{206}Pb/^{238}U$ age are shown in bold in Table 1. Three data points (spot-2, 5 & 8; dotted-line error ellipses in Fig. 5a & b) were excluded from the age calculation because of their high U and very high common Pb values. In addition, spot-10 was excluded from the calculation because it is statistically older, and may represent an area of the zircon with some degree of inheritance. We interpret the mean $^{206}Pb/^{238}U$ age as the time of crystallization for leucogranite vein LGG2; within the limits of analytical error, this age is the same as the one obtained for leucogranite LGG5.

Sample GRG4, a medium-grained biotite granite, was sampled on the southern bank of the Susqueda reservoir (UTM: 457824 4645624). U–Pb data of 12 zircon points gave a mean $^{206}Pb/^{238}U$ age of 305.9 ± 1.5 Ma (Fig. 6c; MSWD = 0.85; 2-sigma). Only one data point (spot-7; dotted-line error ellipse in Fig. 6b) from this sample was excluded from the age calculation because this zircon spot is statistically younger, and may represent initial stages of Pb loss in this particular zircon. We interpret this mean $^{206}Pb/^{238}U$ age as the time of crystallization for the Susqueda biotite granite GRG4.

Sample G04SQ, a fine-grained diorite, was collected near the southern end of the Susqueda dam (UTM: 460601 4647607) from an outcrop showing an igneous banding concordant with the host rocks. U–Pb zircon data for this sample, plotted in a Tera–Wasserburg concordia (Fig. 7a), are very concordant, and nine data points gave a mean $^{206}Pb/^{238}U$ age of 323.6 ± 2.8 Ma (Fig. 7b; MSWD = 1.9; 2-sigma). Only one data point (spot-4; dotted-line error ellipse in Fig. 7a) from this sample was excluded from the age calculation, because this zircon spot was very high U compared to the other concordant zircon grains. There is no evidence of the presence of zircon inheritance in this sample. Individual zircon ages used to calculate the preferred $^{206}Pb/^{238}U$ age are shown in bold in Table 1. We interpret the mean $^{206}Pb/^{238}U$ age as the time of crystallization for the Susqueda diorite.

Fig. 6. Résultats géochronologiques sur zircons du granite à biotite GRG4. (**a**) Représentation de toutes les données obtenues dans le diagramme Tera–Wasserburg concordia U–Pb. (**b**) Détail pour les zircons les plus concordants. (**c**) Diagramme des intervalles d'âges obtenus pour les différents zircons et âge moyen pondéré $^{206}Pb/^{238}U$.

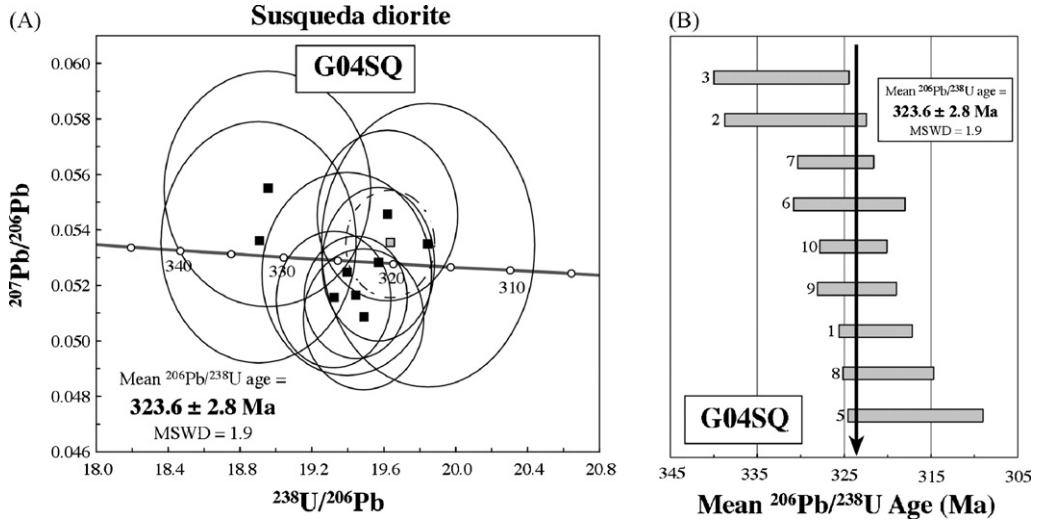

Fig. 7. U–Pb Shrimp-RG zircon geochronology data for the Susqueda diorite (G04SQ). (**a**) Tera–Wasserburg U–Pb concordia plot with solid-line ellipses with black square centres representing the data used for $^{206}Pb/^{238}U$ age calculation. The dotted-line error ellipse with a gray square centre represents a data spot excluded from age calculation (Spot-4). (**b**) Weighted mean $^{206}Pb/^{238}U$ age graph with calculated age and MSWD.

Fig. 7. Résultats géochronologiques sur zircons de la diorite de Susqueda G04SQ. (**a**) Représentation de toutes les données obtenues dans le diagramme concordia U–Pb de Tera–Wasserburg. (**b**) Diagramme des intervalles d'âges obtenus pour les différents zircons et âge moyen pondéré $^{206}Pb/^{238}U$.

3. Geological implications of new U–Pb zircon geochronology: a discussion

This study shows that the Susqueda subconcordant intrusion and its contact-induced melting in the metapelites constituted a specific event that took place at 323.6 ± 2.8 Ma at the Namurian–Visean boundary [4] at ca. 3 kbar and 760 °C [12]. This would also be the age of D2, whatever the meaning (transpressive or transtensive) of the latter is.

This Susqueda diorite would be equivalent in age and probably in meaning to the earliest intrusive ones in the West Asturian Leonese zone in northwestern Iberia [3]. Consequently, D1 must be older, at least Lower Carboniferous, in northeastern Iberia.

The syn-D2 Susqueda intrusion is clearly separated in time from that of the leucogranites (301.5 ± 1.7; 305.3 ± 1.9; 299.0 ± 2.3 Ma) and of the coeval biotite granite (305.9 ± 1.5 Ma). These Westphalian–Stephanian ages are similar to those of the Albères, Querigut [13] Mont-Louis, and La Junquera [9] granitoids, and several others in the Pyrenean axial zone (B. Laumonier, pers. comm.), which have been related to the extensional collapse of the chain D3. Also related to the latter would be the pre- to syn-D3 leucogranites, D2 and D3 hence being separated by around 20 Ma in this part of the chain.

Another interesting consideration is that leucogranites and biotite granites are almost coeval, the former being slightly younger. The age link between both is an unexpected result of this study, and the reason for dating three different leucogranite veins, in an attempt to confirm their age. The presence of andalusite xenocrysts [2] in the leucogranites suggests that these are, at least in part, the melting-induced products of the biotite granites in the host rocks, at a deeper level than that of the present outcropping. This induced melting could have been similar to that which occurred in the contact of the Susqueda complex around 20 Ma earlier, where 15–20% partial melt was formed, restricted to the inner contact rocks [12].

Deformation can be used to constrain the age of the metamorphism in Osor if it is assumed that D2 is the same age in Osor and Susqueda. In this case, the 323.6 ± 2.8 Ma age of the Susqueda diorite would also be the age of the syn-D2 metamorphic peak in Osor. If the baric peak in Osor at around 5 kbar and 660 ± 40 °C [11], near the muscovite dehydration melting, is about the same age, then there is also a 20-Ma gap between the baric peak and the leucogranites (323 Ma vs. 300 Ma). An age gap of 10 to 15 Ma between the metamorphic baric peak and leucogranite formation is observed in the Himalayas [16], where the latter appears to be formed by decompressional melting of the protoliths [10]. However, in the Guilleries massif, given the spatial and temporal relation between the leucogranites and biotite granites, the heat supplied by the latter seems to have played a critical role in leucogranite genesis in a thermal pulse younger than the high-grade metamorphism in Osor and the likely coeval Susqueda intrusion.

There are still two questions that remain open: one is that, unlike in the case of the Susqueda contact rocks, the heat source involved in the widespread low-*P*, high-*T* Osor metamorphism is still unknown; the other is why the late biotite granites induced crustal melting, producing the leucogranites, but there is only limited melting restricted to the contact in the hotter Susqueda diorite and there are no melts linked with the likely coeval sillimanite-grade Osor metamorphism. A hypothetical answer to the latter question would be that Susqueda was intruded in relatively cold middle-crustal rocks, and that melts migrated from the Osor rocks, explaining their restitic signature [11].

Acknowledgements

This work has benefited from the Spanish Research Project CGL2006–09509/BTE. We are grateful to Bernard Laumonier for providing us with granite ages from the Pyrenees, and commenting them on a complete and updated summary. M.L. Arboleya is also thanked for her review of the paper and R. Martínez for his advice on the Time Scale. A. Iriondo is grateful to Joe Wooden, Frank Mazdab, and Brad Ito from the U.S. Geological Survey at Stanford University for their close supervision with zircon-mount preparations and imaging (CL), and with the Shrimp-RG U–Pb zircon analyses and instrument tuning. David Owen from the UAB's 'Servei d'Idiomes' is acknowledged for reviewing the English text. Julien Babault is acknowledged for reviewing the French text. The suggestions made by two referees greatly helped to improve the final version.

Appendix A. Supplementary material

The online version of this article contains additional supplementary material. Please visit at doi:10.1016/j.crte.2007.12.006

References

[1] F. Debon, P. Enrique and A. Autran, Le plutonisme hercynien des Pyrénées, in: A. Barnolas, J.-C. Chiron (Eds.), Synthèse géologique et géophysique des Pyrénées, vol. I, Éditions BRGM–ITGE, 1996, pp. 361–499.

[2] H. Durán, El Paleozóico de les Guilleries, PhD thesis Universitat Autònoma de Barcelona, 1985.

[3] J. Fernandez-Suarez, G.R. Dunning, G.A. Jenner, G. Gutiérrez-Alonso, Variscan collisional magmatism and deformation in NW Iberia: constraints from U–Pb geochronology of granitoids, J. Geol. Soc. Lond. 157 (2000) 565–576.

[4] F.M. Gradstein, J.G. Ogg, A.G. Smith, A Geologic Time Scale 2004, Cambridge University Press, Cambridge, UK, 2004.

[5] G. Guitard, Le métamorphisme hercynien mésozonal et les gneiss œillés du massif de Canigou (Pyrénées orientales), Mem. BRGM 63 (1970) 1–349.

[6] K.L. Ludwig, SQUID, version 1.02, A User's Manual, Berkeley Geochronology Center, Spec. Publ. 2 (2001) 17.

[7] K.L. Ludwig, ISOPLOT, version 3.00, A Geochronological Toolkit for Microsoft Excel: Berkeley Geochronology Center, Spec. Publ. 4 (2003) 70.

[8] F.J. Martínez, M. Julivert, A. Sebastián, M.L. Arboleya, J.I. Gil Ibarguchi, Structural and thermal evolution of high-grade areas in the northwestern parts of the Iberian massif, Am. J. Sci. 288 (1988) 969–996.

[9] O. Maurel, J.-P. Respaut, P. Monié, N. Arnaud, M. Brunel, U–Pb emplacement and $^{40}Ar/^{39}Ar$ cooling ages of the Mont-Louis granite massif (eastern Pyrenees, France), C. R. Geoscience 336 (2004) 1091–1098.

[10] A.E. Patiño-Douce, N. Harris, Experimental constraints of Himalayan anatexis, J. Geol. 39 (1998) 689–710.

[11] J. Reche, F.J. Martínez, Evolution of bulk composition, mineralogy, strain style and fluid flow during an HT–LP metamorphic event: sillimanite zone of the Catalan Coastal Ranges Variscan basement, NE Iberia, Tectonophysics 348 (2002) 111–134.

[12] M. Riesco, K. Stüwe, J. Reche, F.J. Martínez, Silica depleted melting of pelites. A petrogenetic grid with application to the Susqueda Aureole, Spain, J. Metamorph. Geol. 22 (2004) 475–494.

[13] M.-P. Roberts, C. Pin, J.-D. Clemens, J.-L. Paquette, Petrogenesis of mafic to felsic plutonic rock associations: the calc-alkaline Querigut complex, French Pyrenees, J. Petrol. 41 (2000) 809–844.

[14] J.S. Stacey, J.D. Kramers, Approximation of terrestrial lead isotope evolution by a two-stage model, Earth Planet. Sci. Lett. 26 (1975) 207–221.

[15] M. Vilà, C. Pin, P. Enrique, M. Liesa, Telescoping of three distinct magmatic suites in an orogenic setting: Generation of Hercynian igneous rocks of the Albera Massif (eastern Pyrenees), Lithos 83 (2005) 97–127.

[16] J.D. Walker, M.W. Martin, S.A. Bowring, M.P. Searle, D.J. Waters, K.V. Hodges, Metamorphism, melting, and extension: Age constraints from the High Himalayan Slab of Southeast Zanskar and Northwest Lahaul, J. Geol. 107 (4) (1999) 473–495.